Cancer Research

Generation of a Selective Small Molecule Inhibitor of the CBP/p300 Bromodomain for Leukemia Therapy

Sarah Picaud[1,2], Oleg Fedorov[1,3], Angeliki Thanasopoulou[4], Katharina Leonards[4], Katherine Jones[5], Julia Meier[1,3], Heidi Olzscha[6], Octovia Monteiro[1,3], Sarah Martin[1,3], Martin Philpott[1,3], Anthony Tumber[1,3], Panagis Filippakopoulos[1,2], Clarence Yapp[3], Christopher Wells[1,3], Ka Hing Che[7], Andrew Bannister[7], Samuel Robson[7], Umesh Kumar[5], Nigel Parr[5], Kevin Lee[5], Dave Lugo[8], Philip Jeffrey[8], Simon Taylor[8], Matteo L. Vecellio[3], Chas Bountra[1], Paul E. Brennan[1,3], Alison O'Mahony[9], Sharlene Velichko[9], Susanne Müller[1,3], Duncan Hay[3], Danette L. Daniels[10], Marjeta Urh[10], Nicholas B. La Thangue[6], Tony Kouzarides[7], Rab Prinjha[5], Jürg Schwaller[4], and Stefan Knapp[1,3]

Abstract

The histone acetyltransferases CBP/p300 are involved in recurrent leukemia-associated chromosomal translocations and are key regulators of cell growth. Therefore, efforts to generate inhibitors of CBP/p300 are of clinical value. We developed a specific and potent acetyl-lysine competitive protein–protein interaction inhibitor, I-CBP112, that targets the CBP/p300 bromodomains. Exposure of human and mouse leukemic cell lines to I-CBP112 resulted in substantially impaired colony formation and induced cellular differentiation without significant cytotoxicity. I-CBP112 significantly reduced the leukemia-initiating potential of MLL-AF9$^+$ acute myeloid leukemia cells in a dose-dependent manner *in vitro* and *in vivo*. Interestingly, I-CBP112 increased the cytotoxic activity of BET bromodomain inhibitor JQ1 as well as doxorubicin. Collectively, we report the development and preclinical evaluation of a novel, potent inhibitor targeting CBP/p300 bromodomains that impairs aberrant self-renewal of leukemic cells. The synergistic effects of I-CBP112 and current standard therapy (doxorubicin) as well as emerging treatment strategies (BET inhibition) provide new opportunities for combinatorial treatment of leukemia and potentially other cancers. *Cancer Res; 75(23); 5106–19. ©2015 AACR.*

Introduction

The cAMP responsive element binding protein (CREB)-binding protein (CBP; CREBBP) and p300 (adenovirus E1A-associated 300-kD protein) are two closely related and evolutionary conserved histone acetyl transferases (HAT; ref. 1). CBP/p300 function as transcriptional regulators by acetylating histone tails and other nuclear proteins. They also act as scaffolds recruiting transcription factors to transcriptional active loci through a large diversity of protein interaction domains. The HAT activity of CBP is regulated by autoacetylation of a basic surface loop region that competes with substrate binding and by the presence of a RING domain located adjacent to the catalytic HAT domain (2). Interestingly, CBP/p300-mediated acetylation creates binding sites for the acetyl-lysine–specific CBP/p300 bromodomain, which is required for proper substrate targeting, resulting in a positive feedback loop and maintenance of CBP/p300 enzymatic activity (2).

Homozygous loss of either *Cbp* or *p300* leads to embryonic lethality *in utero* in mice due to developmental defects including impaired hematopoiesis (3, 4). Studies in heterozygous mice have characterized *Cbp* as an essential regulator of hematopoietic stem cell (HSC) self-renewal. Likewise, conditional ablation of *Cbp* in adult mice altered differentiation, quiescence, apoptosis, and self-renewal of adult HSCs (5).

CBP/p300 has been functionally linked to the development of multiple human cancers, including solid tumors and hematologic

[1]Nuffield Department of Clinical Medicine, Structural Genomics Consortium, University of Oxford, Oxford, United Kingdom. [2]Nuffield Department of Clinical Medicine, Ludwig Institute for Cancer Research (LICR), University of Oxford, Oxford, United Kingdom. [3]Nuffield Department of Clinical Medicine, Target Discovery Institute (TDI), University of Oxford, Oxford, United Kingdom. [4]Laboratory of Childhood Leukemia, Department of Biomedicine, University of Basel and Basel University Children's Hospital, Basel, Switzerland. [5]Epinova DPU, Immuno-Inflammation Therapy Area Unit, Medicines Research Centre, GlaxoSmithKline, Stevenage, United Kingdom. [6]Laboratory of Cancer Biology, Department of Oncology, Medical Sciences Division, University of Oxford, Oxford, United Kingdom. [7]Gurdon Institute and Department of Pathology, University of Cambridge, Cambridge, United Kingdom. [8]Experimental Medicines Unit, Medicines Research Centre, GlaxoSmithKline, Stevenage, United Kingdom. [9]BioSeek Division of DiscoveRx Corporation, South San Francisco, California. [10]Promega Corporation, Madison, Wisconsin.

Note: Supplementary data for this article are available at Cancer Research Online (http://cancerres.aacrjournals.org/).

S. Picaud, O. Fedorov, A. Thanasopoulou, and K. Leonards contributed equally to this article.

Corresponding Authors: Stefan Knapp, Goethe-University Frankfurt, Institute for Pharmaceutical Chemistry, Max-von Laue Str. 9, 60438 Frankfurt am Main, Germany. Phone: 49-0-69-798-29871; Fax: 49-0-69-798-12799; E-Mail: knapp@pharmchem.uni-frankfurt.de; and Jürg Schwaller, Laboratory of Childhood Leukemia, Department of Biomedicine and Children's Hospital, University of Basel, Basel, Switzerland. E-mail: j.schwaller@unibas.ch

doi: 10.1158/0008-5472.CAN-15-0236

malignancies (6). CBP/p300 has been detected in several oncogenic fusions in leukemia involving either the MOZ acetyltransferase or the mixed linage leukemia (MLL) gene product promoting cell proliferation (7, 8). The most prevalent is the chromosomal translocation t(11;16)(q23;p13) associated with mostly therapy-related acute myeloid leukemia (AML) or myelodysplastic syndromes resulting in a fusion protein that contains the bromodomains of CBP and parts of MLL (8, 9). CBP/p300 was also proposed to act as transcriptional coactivator of other leukemogenic proteins such as the NUP98-HOXA9 fusion (10). Recently, it has been shown that p300 interacts with the AML1-ETO fusion protein, present in over 20% of human AML, and that it regulates transcription of multiple AML1–ETO target genes including Id1 (inhibitor of DNA binding 1), the cell-cycle inhibitor p21 and Egr1 (early growth response 1) that are drivers of self-renewal of hematopoietic stem/progenitor cells (11). Furthermore, inhibition of p300 abrogates acetylation of AML1-ETO and impaired clonogenic growth *in vitro* and leukemic transformation *in vivo* (12).

The multidomain organization of CBP/p300 has prompted several inhibitor development projects. The HAT activity has been targeted by natural compounds that mostly lacked specificity (13). The most potent HAT inhibitor developed so far is C646, which has low micromolar activity (14). C646 inhibits growth of tumor cell lines and promotes cellular senescence and reduced colony formation of AML1-ETO–positive AML cell lines and primary blasts isolated from leukemic mice and AML patients (15). In addition, "ischemin" and a number of nonspecific fragments with micromolar potency have been reported to target the CBP bromodomain (16, 17).

Here, we report a selective and highly potent chemical probe compound targeting the bromodomains of CBP/p300. Bromodomains are protein interaction domains with predicted good druggability (18), which has been demonstrated by potent and selective inhibitors developed for the BET (bromo and extracellular domain) family of transcriptional regulators (19–22). We developed the acetyl-lysine mimetic oxazepine inhibitor I-CBP112 that binds to CBP/p300 with nanomolar affinity and good selectivity. In leukemia, we found that I-CBP112 impaired the disease-initiating self-renewal leukemic cells *in vitro* and *in vivo* without causing significant cytotoxicity.

Materials and Methods

Protein purification

cDNA encoding human bromodomains were cloned, expressed, and purified as previously described (19). For purification of *in vivo* biotinylated protein expression, the same construct boundaries (e.g., CBP residues R1081-G1198) were bromodomain subcloned into pNIC-BIO1 vector, a derivative from pNIC28-Bsa4 vector (Gene Bank: EF198106) containing a 10 His-tag and TEV protease cleavage site at the N-terminus and an in frame biotinylation sequence (SSKGGYGLNDIFEAQKIEWHE) inserted at the C-terminus. The constructs were transformed into BL21 (DE3)-R3-BirA cell line (BL21 derivative coexpressing BirA using a pACYC coexpression vector). Cells were grown overnight at 37°C in 10 mL of Luria-Bertani medium with 50 μg/mL kanamycin and 34 μg/ml chloramphenicol. The start-up culture was diluted 1:1000 in fresh medium and cell growth was allowed at 37°C to an optical density of about ∼1.0 (OD_{600}) before the temperature was decreased to 25°C. D-Biotin was dissolved into 10 mM bicine pH8.3 and added to the culture at 500 μM final. The protein expression was induced for 8 hours at 25°C with 50 μM isopropyl-β-D-thiogalactopyranoside. Proteins were purified using Ni-affinity chromatography and size exclusion chromatography.

Thermal shift assay

Thermal melting experiments were carried out using an Mx3005p Real-Time PCR machine (Stratagene) as described (23). Proteins were buffered in 10 mM HEPES pH 7.5, 500 mM NaCl, and assayed in a 96-well plate at a final concentration of 2 μM in 20 μL volume. Compounds were added at a final concentration of 10 μM. SYPRO Orange (Molecular Probes) was added as a fluorescence probe at a dilution of 1:1000.

AlphaScreen assay

Assays were performed as described previously (24), with minor modifications from the manufacturer's protocol (PerkinElmer). A 11-point 1:2.5 serial dilution of the ligands was prepared over the range of 5000–0 μM and 0.1 μL transferred to low-volume 384-well plates filled with 5 uL of the assay buffer (ProxiPlate-384 Plus, PerkinElmer), followed by 7 uL of biotinylated peptide H-ALREIRRYQK(ac)STELLIRKLK(biotin)-OH and His-tagged protein to achieve final assay concentrations of 50 nM. Plates were sealed and incubated for a further 30 minutes before the addition of 8 μl of the mixture of streptavidin-coated donor beads (12.5 μg/ml) and nickel chelate acceptor beads (12.5 μg/ml) under low light conditions.

Cell culture and reagents

Human cell lines (MOLM13, MONOMAC, THP1, KOCL45, RS4;11, SEM, MV4;11, KOCL44, KOPN8, KASUMI-1, MUTZ5, HL60, K562, PL21, REH, U937) were obtained from ATCC and the Leibnitz Institute DSMZ-German Collection of Microorganisms and Cell Cultures (www.dsmz.de). Cell lines were cultured in RPMI-1640 medium (Sigma) containing 10% fetal bovine serum, 100 U/ml penicillin, and 100 U/ml streptomycin (Gibco). Synthesis of I-CBP112 and related analogues will be described elsewhere. The inhibitor was dissolved in DMSO at a concentration of 10 mM and diluted further in culture medium RPMI-1640 immediately before use.

I-CBP112 in an *in vivo* model of MLL-AF9+ leukemia

Leukemic blasts expressing MLL-AF9 were treated in liquid culture with 5 μM of I-CBP112 for 3 days. Control cells were exposed to the corresponding concentration of the DMSO vehicle. The 50×10^3 treated cells were then transplanted into sublethally irradiated (600Rad) syngeneic mice via tail vein injection. Upon the development of signs of disease, the mice were sacrificed and analyzed. All experiments were done according to Swiss laws for animal welfare and approved by the Swiss Cantonal Veterinary Office of Basel (Basel, Switzerland).

RNA preparation and gene expression profiling

KASUMI-1, SEM, and MOLM13 cells were treated with 3 ìM of I-CBP112 or the DMSO vehicle for 4 days. On the third day of treatment, the cells were replated in fresh medium with or without the inhibitor. Total RNA was extracted using the RNA extraction kit (Macherey-Nagel, GmbH & Co.) according to the manufacturer's protocol. Primers for q-PCR and chromatin immunoprecipitation (ChIP) analysis are provided in the Supplementary Methods.

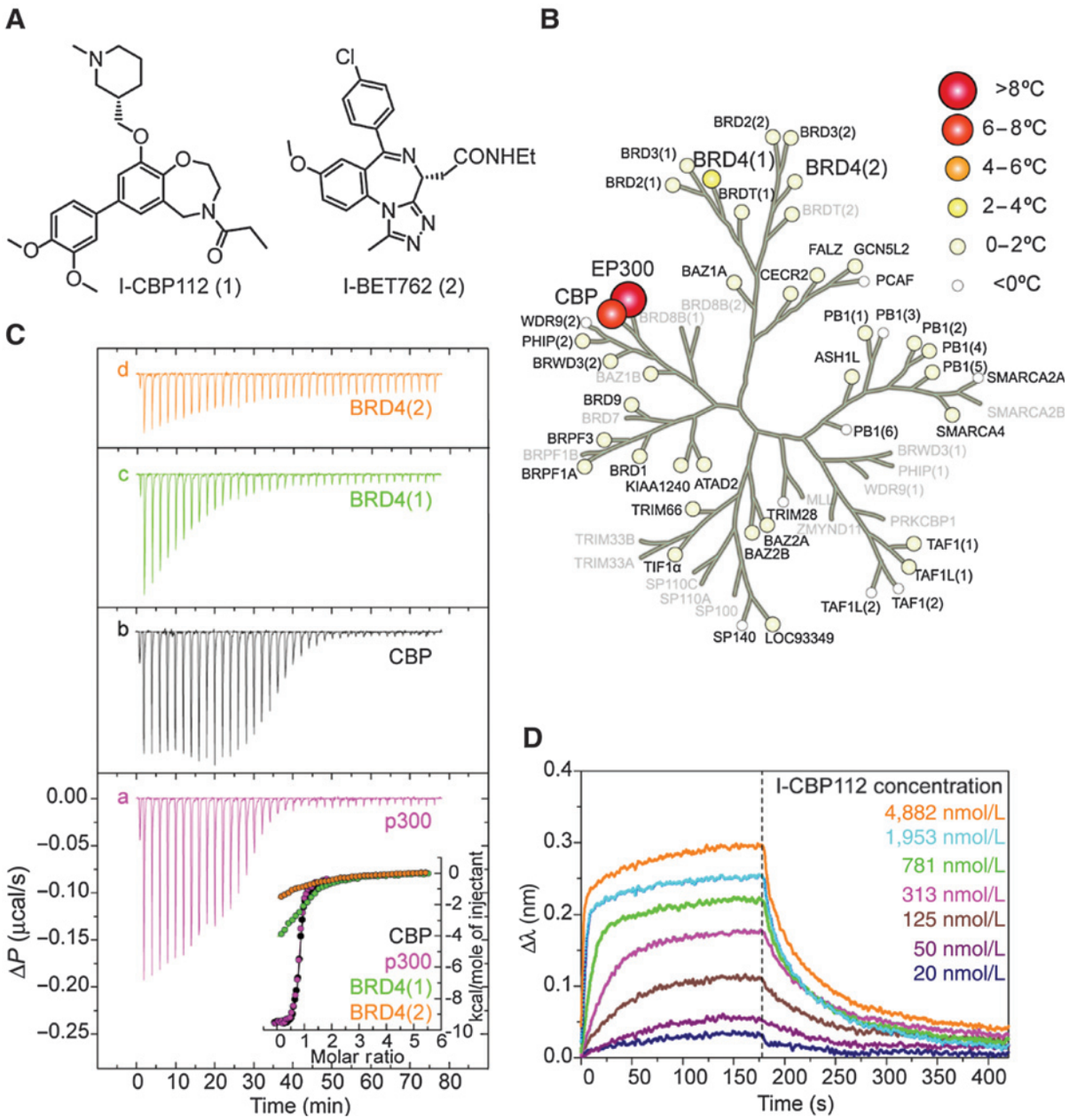

Figure 1.
In vitro characterization of I-CBP112. A, chemical structure of I-CBP112 and the BET inhibitor I-BET762. B, selectivity of I-CBP112 assessed by temperature shift data. Temperature shifts are shown as spheres as indicated in the figure and were mapped to the phylogenetic tree of the bromodomain family. Screened targets are labeled in black and targets that were not screened are shown in gray. C, isothermal titration calorimetry titration for the bromodomain of CBP (a), p300 (b), and bromodomains BRD4(1) (c), and BRD4(2) (d), respectively. Shown are raw titration heats (top) as well as binding isotherms shown as normalized binding heats (bottom). Nonlinear least squares fits to the data are shown as solid lines and fitted parameters are included in Supplementary Table S2. D, concentration dependent sensograms (BLI) of I-CBP112 binding to CBP.

Primary human blasts

Peripheral blood samples were collected with informed consent from patients with newly diagnosed or relapse AML. Mononuclear cells were separated by Ficoll-Histopaque and frozen in 10% DMSO. Cells were then used for colony formation assays, as described above.

Drug synergism

KASUMI-1, SEM, and MOLM13 cells were plated in a 9-well plate and treated with iCBP112 combined with doxorubicin or JQ1 in cytotoxicity assays. Eight different concentrations of iCBP112 and 15 of JQ1 and doxorubicin were used in ratios from 8:1 to 1:16 (Supplementary Fig. 12A). As 1X, we set

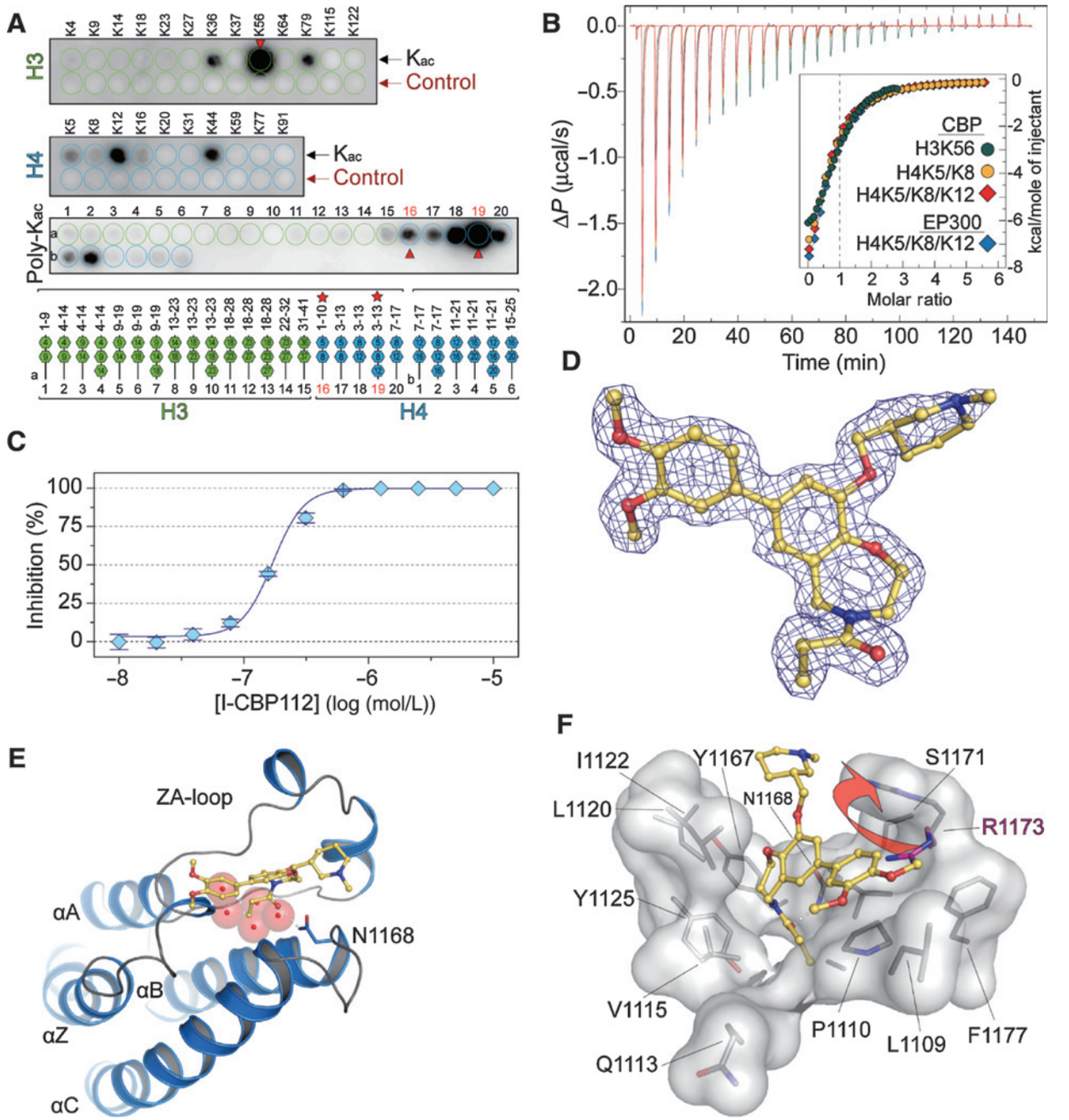

Figure 2.
Recognition of acetylated peptide by CBP and structural features of I-CBP112 interaction with the CBP bromodomain. A, SPOT analysis of the binding of CBP to a library of acetylated histone peptides. The row labeled "control" represents the corresponding nonacetylated peptides. The positions of the polyacetylation sites are indicated at the bottom. Peptides used for ITC experiments are highlighted by red stars and arrows on the plot. B, ITC experiments measuring binding affinities of identified mono- and polyacetylated peptides. C, determination of *in vitro* IC_{50} value for the CBP/I-CBP112 interaction using AlphaScreen and the $H3K56_{ac}$ peptide. D, $2F_oF_c$ electron density map defining the conformation and binding mode of the I-CBP112 inhibitor in complex with CBP. E, cocrystal structure of the bromodomain of CBP in complex with I-CBP112. Shown is a structural overview using a ribbon diagram. The main structural elements are labeled. The inhibitor is shown as a stick model. Hydrogen bonds are indicated by dotted lines and water molecules are show as red semitransparent spheres. F, details of the I-CBP112 interaction with the CBP bromodomain. Binding of the inhibitors induces an outward movement of R1173 that is indicated by an arrow.

approximately the IC_{50} concentration. After excluding the concentrations that gave either no effect or extreme effect for the single treatment (Supplementary Fig. 13), we ran the CompuSyn software and calculated the combination index (CI) value using the Chou-Talalay method, where CI<1 indicates synergism.

Crystallization and structure solution

Aliquots of the purified proteins were set up for crystallization using a mosquito crystallization robot (TTP Labtech). Coarse screens were typically set up onto Greiner 3-well plates using three different drop ratios of precipitant to protein per condition (100+50 nL, 75+75 nL, and 50+100 nL). All crystallizations were carried out using the sitting drop vapor diffusion method at 4°C. CBP crystals with I-CBP112 (2 mM final concentration) were grown by mixing 200 nL of the protein (8.6 mg/ml) with 100 µL of reservoir solution containing 0.10 M $MgCl_2$, 0.1 M MES pH 6.0, 20% PEG 6K, and 10% ethylene glycol. Crystals were cryo-protected using the well solution supplemented with additional ethylene glycol and were flash frozen in liquid nitrogen. Data were collected at diamond beamline I04 at a wavelength of 1.0121 Å. Phases were obtained by molecular replacement using an ensemble of known bromodomain models (PDB IDs 2OSS, 2OUO, 2GRC, 2OO1, 3DAI, 3D7C, 3DWY). The models and structure factors have been deposited with PDB accession codes: 4NR6. Additional experimental details are available in Supplementary Data.

Results

Discovery of I-CBP112

On the basis of the reported weak CBP/p300 bromodomain binding activity of BET inhibitors such as JQ1 and I-BET762 we analyzed the CBP/p300 activity of a series of related compounds that all contained a benzo-oxazepine core structure (Fig. 1A). Hit expansion at several positions led to I-CBP112 with good activity against CBP/p300. The description of the structure activity relationship (SAR) of this compound class as well as the synthesis of I-CBP112 and its intermediates will be reported elsewhere.

I-CBP112 is a potent and selective CBP/p300 inhibitor

We used temperature shift assays for the characterization of I-CBP112 potency and selectivity within the bromodomain family. This assay monitors binding of an inhibitor to a protein based on the magnitude of temperature stabilization (23). I-CBP112 showed significant stabilization of CBP/p300 melting temperatures (7.8°C and 8.6°C, respectively) while ΔT_m values were low for 41 other members of the human bromodomain family suggesting excellent selectivity of the developed inhibitor (Fig. 1B; Supplementary Table S1). We investigated I-CBP112 selectivity further using biolayer interferometry (BLI) as an additional selectivity screening technology. Similar to the related surface plasmon resonance, this technology measures interactions of ligands with biomolecules immobilized on a surface monitoring changes in refractive index. To confirm the selectivity of I-CBP112, we screened a panel of 42 representative bromodomains that were homogenously biotinylated *in vivo* during recombinant expression. BLI confirmed the excellent selectivity measured by temperature shift experiments identifying only bromodomains of the BET family members as having weak off-target activity (Supplementary Fig. S1). Finally, we determined affinity of I-CBP112 for CBP/p300 in solution using isothermal titration calorimetry

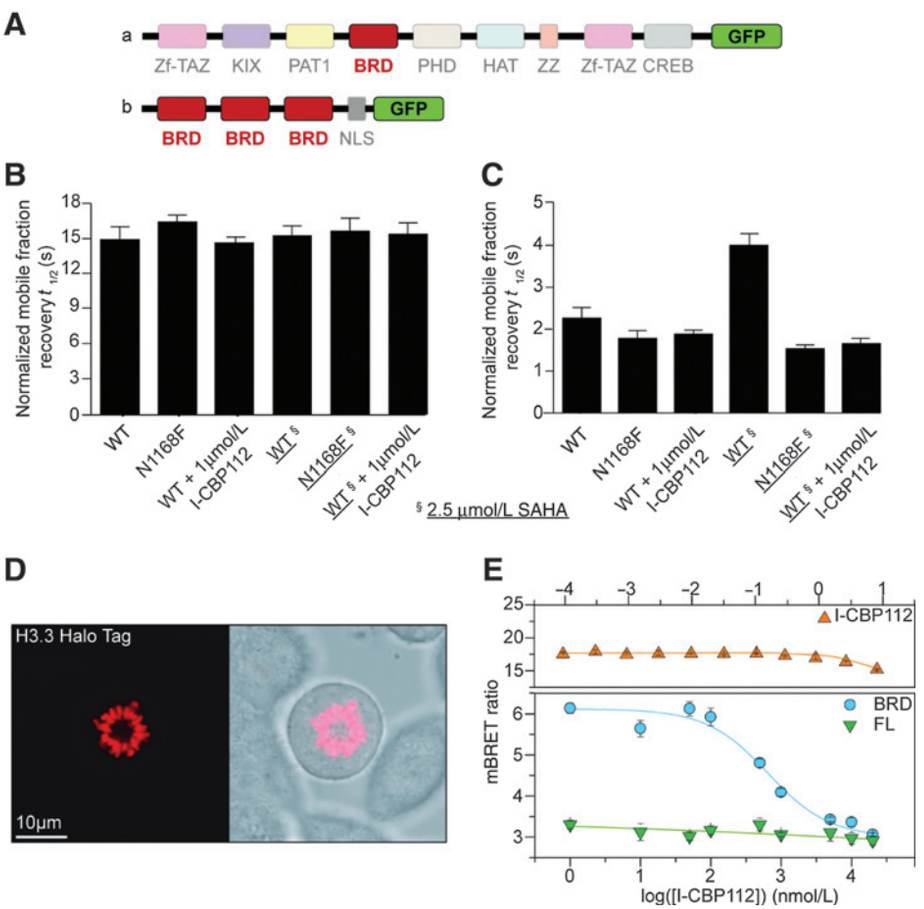

Figure 3.
I-CBP112 displaces the CBP bromodomain from chromatin. A, domain organization of full length CBP (top) and of the 3xCBP_{BRD}/GFP construct used (bottom). B, FRAP experiment showing half-recovery times for full length CBP/GFP and its inactivating mutant N1168F. C, FRAP experiment showing half-recovery times of the fluorescent signal of 3xCBP_{BRD}/GFP (WT) and its inactivating mutant 3xBRD^{N1168F}_{CBP}/GFP. Experiments with SAHA-treated cells (2.5 µmol/L) are indicated by underlined constructs. D, fluorescent image (left) and phase contrast image (right) of metaphase chromosomes of Halo-tagged histone H3.3-transfected HEK293T cells showing incorporation of the tagged histone into chromatin. E, NanoBRET experiments showing the dose response of NanoLuc Luciferase fusion full-length CBP and the isolated CBP bromodomain. The construct containing only the bromodomain was readily displaced by I-CBP112 with a cellular IC_{50} value of 600 ± 50 nmol/L. No displacement was observed using full-length GFP-BRD4 in agreement with the *in vitro* selectivity of I-CBP112 (top).

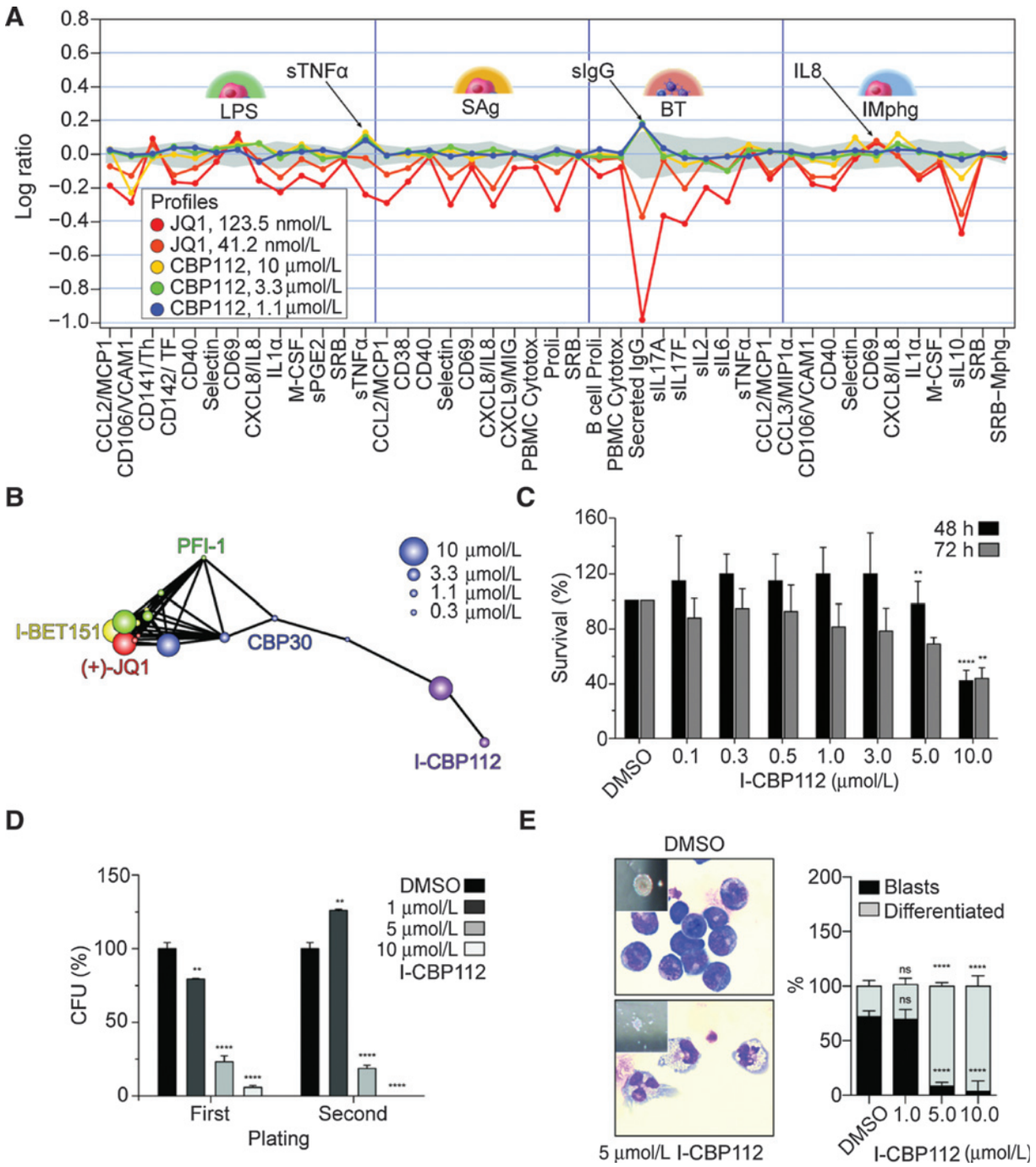

Figure 4.
BioMAP data for I-CBP112 and effects on mouse MLL-CBP–immortalized bone marrow cells. A, BioMAP data of four hematopoietic coculture systems (Sag and LPS, peripheral blood mononuclear cells cultured with venular endothelial cells; BT, B cells and peripheral blood mononuclear cells; IMphg, venular endothelial cells cocultured with M1 macrophages) treated with JQ1 or I-CBP112. The full BioMAP and explanation of the monitored marker proteins is shown in Supplementary Fig. S2. B, correlation of the phenotypic response of the panBET inhibitors JQ1, PFI-1, IBET-151, CBP30, and I-CBP112. Responses to compound inhibition above the selected threshold (Pearson ≥ 0.6) are represented by connected dots. C, cytotoxicity (WST1 assay) of I-CBP112 on murine bone marrow cells immortalized by retroviral expression of the MLL-CBP fusion oncogene. Shown is the mean percentage normalized to vehicle-treated control; error bars represent ±SD; *P* values were calculated by using ANOVA and Dunnett multiple comparison; **, $P < 0.01$; ****, $P < 0.0001$; $n = 4$. D, clonogenic growth and replating assay of mouse MLL-CBP immortalized bone marrow-derived murine progenitors in methylcellulose, treated with I-CBP112. Shown is the mean percentage normalized to vehicle-treated control; error bars represent ±SD; *P* values were calculated by using ANOVA and Dunnett multiple comparison; **, $P < 0.01$; ****, $P < 0.0001$; $n = 2$. E, morphologic changes of MLL-CBP immortalized progenitors on cellular and colony level upon exposure to increasing concentrations of CBP112 (left). Percentage of blasts and differentiated cells scored on cytospots. Shown is the mean percentage normalized to vehicle-treated control; error bars represent ±SD; *P* values were calculated by using ANOVA and Dunnett multiple comparison; ****, $P < 0.0001$; $n = 20$ scored high-magnification (×60) fields (right).

(ITC), which resulted in determination of a dissociation constant (K_d) of 151 ± 6 nmol/L and 167 ± 8 nmol/L for CBP and p300, respectively (Fig. 1C; Supplementary Table S2). Dose-dependent BLI experiments resulted in a comparable K_d value for CBP (K_d: 142 nmol/L; Fig. 1D). The most significant off-target activity in our selectivity screen was against BRD4, which showed a ΔT_m of 2.1°C and 0.6°C for the first [BRD4(1)] and second [BRD4(2)] bromodomain, respectively. ITC titrations resulted in the determination of K_ds of 5.6 μmol/L and 20 μmol/L for BRD4(1) and BRD4(2), demonstrating 37 and 132 fold selectivity, respectively (Fig. 1C; Supplementary Table S2).

To assess selectivity of I-CBP112 outside the bromodomain family, we screened both stereoisomers against a commercial selectivity panel including 104 binding assays monitoring binding to nuclear receptors, ion channels, and 32 enzyme assays (including 10 kinases, 9 proteases, and 5 phosphodiesterases). Both I-CBP112 stereoisomers showed similar behavior when screened against this panel that revealed only weak interaction with two GPCRs (α1A and 5HT1) in the low micromolar region (Supplementary Table S3). The *S*-isomer was selected as chemical probe compound and was used in all subsequent cellular assays.

I-CBP112 is an acetyl-lysine competitive inhibitor

To establish a functional assay we studied the specificity of the CBP bromodomain towards histone peptide target sequences by synthesizing acetylated and nonacetylated histone peptides on a SPOT cellulose array (19). We found that the CBP bromodomain did not bind nonacetylated control peptides confirming high specificity for the acetyl-lysine modification (Fig. 2A). The peptide screening data revealed strong interaction of CBP with the histone-3 acetylated lysine 56 ($H3K56_{ac}$), a CBP HAT substrate site, as well as interaction with $H3K36_{ac}$ and $H3K79_{ac}$ and $H4K12_{ac}$ and $H4K44_{ac}$. Polyacetylation seemed to increase binding for some of the histone H4 acetylation marks. However, ITC data showed that the CBP bromodomain had similar affinities for mono- and diacetylated peptides and the determined stoichiometries of 0.5 for polyacetylated peptides suggested that two bromodomains simultaneously bound one diacetylated peptide supporting a canonical binding model in which one acetyl-lysine interacted with one CBP bromodomain (Fig. 2B; Supplementary Table S4). The strongest interaction was observed with $H3K56_{ac}$ (K_d = 13.8 μmol/L), which was used for the development of an Amplified Luminescence Proximity Homogeneous Assay (AlphaScreen; ref. 24). However, we find it likely that additional interaction with acetylation sites other than $H3K56_{ac}$ may occur in the context of intact chromatin in cells. The developed assay demonstrated that I-CBP112 is an acetyl-lysine–competitive inhibitor displacing $H3K56_{ac}$ from the CBP-binding site with an IC_{50} value of 170 nmol/L (Fig. 2C).

Cocrystallization of the *R*-isomer of I-CBP112 with the bromodomain of CBP confirmed the acetyl-lysine mimetic nature of this inhibitor. The structure of the complex was refined at 1.6 Å resolution (Supplementary Table S5). The inhibitor was well defined by electron density allowing assignment of its binding mode (Fig. 2D). As expected, the carbonyl group branching off the oxazepine ring acted as an acetyl-lysine mimetic moiety forming a hydrogen bond with the conserved asparagine (N1168 in CBP) as well as a water-mediated hydrogen bond with Y1125. The five water molecules that are typically present in bromodomain inhibitor and substrate complexes (25) were also conserved in the I-CBP112/CBP complex (Fig. 2E). Surprisingly, I-CBP112 bound with an induced fit binding mode, leading to an outward movement of the side chain of R1173. This movement creates a deep pocket that accommodates the dimethoxyphenyl ring system forming an aromatic stacking interaction with the R1173 side chain (Fig. 2F).

CBP remains bound to chromatin in the presence of I-CBP112

We next investigated whether I-CBP112 could dissociate CBP from chromatin using a fluorescent recovery after photo bleaching (FRAP) assay (26). Full-length CBP contains a large number of protein and DNA interaction domains (Fig. 3A). FRAP measurements using a GFP-tagged full-length CBP construct did not lead to decreased recovery times when treated with I-CBP112, or when a conserved key residue for acetyl-lysine interaction (N1168) was mutated to phenylalanine (N1168F), indicating that full-length CBP cannot be displaced from chromatin by bromodomain inhibitors (Fig. 3B). We used the pan-HDAC inhibitor SAHA to increase chromatin acetylation levels. In agreement with FRAP data using I-CBP112 and site-directed mutants, SAHA treatment did not significantly influence fluorescent recovery times of full-length CBP, suggesting that tight chromatin association of CBP is not exclusively acetylation-dependent and is primarily mediated by interaction domains other than the bromodomain. To verify that I-CBP112 bound to the CBP bromodomain in nuclei of cells, we cloned the CBP bromodomain fused to a nuclear localization signal and a GFP tag. The assay window obtained for this construct was small, which was expected considering the low affinity of isolated bromodomain with acetylated histone tails. However, expression of three bromodomains ($3xCBP^{BRD}$/GFP) fused in frame by a linker region resulted in a GFP fusion protein that showed significant increase in FRAP signal after SAHA treatment and provided a sufficient assay window when compared with the N1168F-mutant construct. Exposure to 1 μmol/L I-CBP112 significantly reduced FRAP signal after SAHA treatment demonstrating that I-CBP112 can indeed target the CBP bromodomain in the nucleus and is capable of competing with acetyl-lysine–mediated interactions of the CBP bromodomain in cellular environments (Fig. 3C). Representative data of beached nuclei as well as normalized fluorescent recovery data are shown in Supplementary Fig. S2. We confirmed these observations by a bioluminescence resonance energy transfer (BRET) assay using NanoLuc Luciferase fusions of full-length CBP and the isolated CBP bromodomain as well as Halo-tagged Histone H3.3, which was readily incorporated into chromatin (Fig. 3D), as BRET pairs. In agreement with our FRAP experiments, dose response experiments revealed that I-CBP112 had no significant effect on the recruitment of full-length CBP to chromatin, whereas a construct containing the bromodomain was readily replaced with a cellular IC_{50} value of 600 ± 50 nmol/L (Fig. 3E) confirming cellular activity of I-CBP112 inhibiting acetylation-dependent CBP bromodomain-mediated interactions.

Phenotypic responses of CBP/p300 bromodomain inhibition

To get insight on the wider consequences of CBP/p300 bromodomain inhibition in cellular systems, we exposed a panel of 12 stimulated primary human cocultured cell types (BioMAP) with I-CBP112 and monitored a broad array of protein biomarkers. This unbiased approach has been well established to assess target-specific phenotypic responses by proving a phenotypic fingerprint of an inhibitor based on a large number of marker

proteins (27). For I-CBP112, the analysis of BioMAP data revealed a modest but robust response on the expression of some of the measured protein markers. Comparison with fingerprints generated by well-established BET bromodomain inhibitors, I-CBP112 revealed a very distinct phenotypic response (Fig. 4A and Supplementary Fig. S3). Some effects of cytokine expression were shared between BET and CBP/p300 inhibitors. Expression of the anti-inflammatory cytokine IL10 or the vascular cell adhesion protein 1 (VCAM1/CD106) for instance was downregulated by both I-CBP112 as well as the BET inhibitor JQ1. In contrast to BET inhibition, I-CBP112 had no effect on expression levels of a number of marker proteins including for instance the chemokine (C-C motif) ligand 2 (CCL2) or the cell adhesion molecule Selectin (CD62). In addition, we observed a number of differential responses comparing both inhibitors. Secreted IgG was for instance strongly downregulated by the BET inhibitor JQ1, but it was upregulated by I-CBP112. Using statistical methods comparing profile similarity, we found that the BET bromodomain inhibitors JQ1, PFI-1, and I-BET151 clustered closely together (Pearson $\geq$ 0.6) in agreement with their reported selectivity for

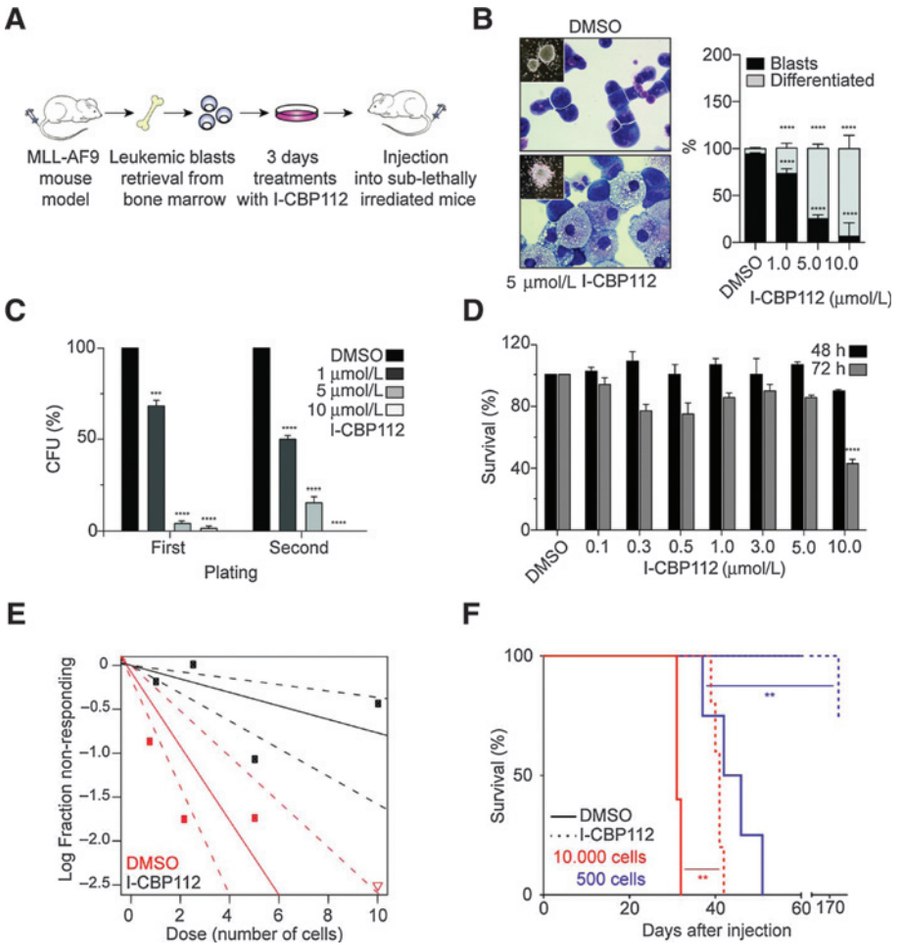

Figure 5.
I-CBP112 impairs self-renewal and disease induction of murine MLL-AF9–driven acute leukemia. A, schematic outline of the used mouse model. Transplanting bone marrow cells retrovirally expressing the MLL-AF9 fusion oncogene leads to AML. Leukemic blasts from diseased mice were *ex vivo* treated with 5 µmol/L of I-CBP112 or DMSO vehicle for 3 days and transplanted into syngeneic secondary recipients. B, changes on cell morphology and colony formation of murine MLL-AF9 leukemic blasts treated with I-CBP112 at different concentrations as indicated in the figure (left). Percentage of blasts and differentiated cells scored on cytospots. Shown is the mean percentage normalized to vehicle-treated control; error bars represent ±SD. *P* values were calculated by using ANOVA and Dunnett multiple comparison; ****, $P < 0.0001$; $n = 20$ scored high-magnification (×60) fields (right). C, clonogenic growth and replating assay of leukemic MLL-AF9 blasts treated with I-CBP112. Concentration as indicated in the figure. Shown is the mean percentage normalized to vehicle-treated control; error bars represent ±SD. *P* values were calculated by using ANOVA and Dunnett multiple comparison; ***, $P < 0.001$; ****, $P < 0.0001$; $n = 2$. D, cytotoxicity (WST1 assay) of leukemic MLL-AF9 blasts treated with I-CBP112. Shown is the mean percentage normalized to vehicle-treated control; error bars represent ±SD. *P* values were calculated by using ANOVA and Dunnett multiple comparison; ****, $P < 0.0001$; $n = 4$. E, extreme limiting dilution analysis (ELDA). Shown is a log-fraction plot of the limiting dilution model fitted to the data. The slope of the line represents the log-active cell fraction. The dotted lines indicate the 95% confidence interval. The data value with zero negative response at highest dose (10 plated cells) is represented by a downpointing triangle. The estimated stem cell frequency decreased from 1/2.3 to 1/13. Statistical significance was assessed by an overall test for differences with $\chi^2$18.3 and DF 1 showing $P < 0.00001$. F, Kaplan–Meier diagram showing significantly extended survival of mice injected with different number of I-CBP112–treated cells (dotted lines) compared with vehicle-treated controls (solid lines). The number of injected cells were 10, 000 cells (red) and 500 cells (magenta). *P* values were calculated using log-rank (Mantel–Cox) test; $n = 4/5$ per group. Survival data for injections of 50,000 cells and 5,000 cells have been included in the Supplementary Data.

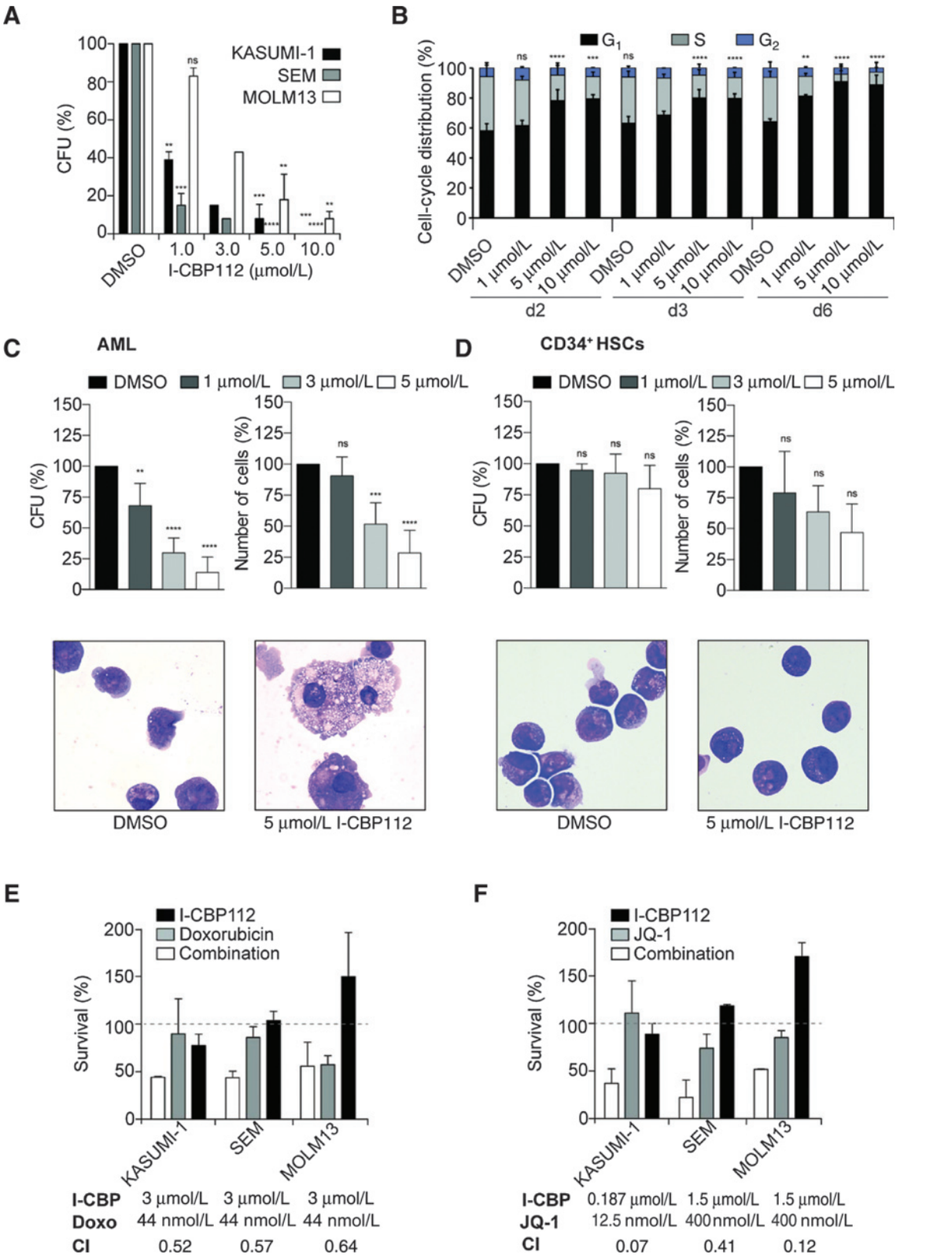

Figure 6.

I-CBP112 impairs the clonogenic growth of human leukemic cells and sensitizes them to BET inhibition and doxorubicin. A, clonogenic activity of three human leukemic cell lines in methylcellulose exposed to different doses of I-CBP112. Shown is the mean percentage normalized to vehicle treated; error bars, ±SD. *P* values were calculated by using ANOVA and Dunnett multiple comparison; **, $P < 0.01$; ***, $P < 0.001$; ****, $P < 0.0001$; $n = 3$. (*Continued on the following page.*)

BET bromodomains. I-CBP112 in contrast showed a distinct phenotypic response (Fig. 4B). Interestingly, another bromodomain inhibitor that we developed recently, CBP30, that has potent *in vitro* activity for the CBP/p300 bromodomain but also significant BET activity (28) clustered with I-CBP112 at low concentration but showed a clear BET bromodomain signature at 10 μmol/L as expected from its dual activity. Thus, exposure of the BioMAP primary cell panel to I-CBP112 resulted in a unique response on cytokine and marker protein expression.

I-CBP112 impairs clonogenic growth of immortalized murine bone marrow cells

Next, we aimed to explore the anticancer potential of I-CBP112 in a CBP/p300-dependent transformation model. Chromosomal translocations have been observed in patients after therapy with topoisomerase inhibitors leading to MLL-CBP fusion proteins that include the bromodomain. Expression of MLL-CBP has been shown to immortalize mouse bone marrow cells *in vitro* but it has a limited capacity of inducing leukemia *in vivo* (29). To address the effect of I-CBP112 on MLL-CBP–driven transformation we therefore established an immortalized hematopoietic cell line by retroviral expression of the MLL-CBP fusion in lineage marker depleted mouse bone marrow cells and expansion by two rounds of replating in methylcellulose. Interestingly, exposure of these cells with I-CBP112 did not affect cell survival and significant cytotoxicity was only observed at high inhibitor concentrations and after prolonged exposure (Fig. 4C). However, exposure to the inhibitor significantly reduced clonogenic growth of MLL-CBP immortalized cells in methylcellulose, which became even more apparent upon replating of the cells (Fig. 4D). I-CBP112 exposure resulted in morphologic changes from large round compact, so called class I type, to smaller and more loosely shaped colonies. Wright–Giemsa–stained cytospots of treated cells harvested from methylcellulose revealed morphologic changes, indicating differentiation of MLL-CBP–immortalized cells (Fig. 4E).

I-CBP112 pretreatment of MLL-AF9$^+$ murine AML blasts reduced the number of LICs and delayed induction of the disease upon transplantation into irradiated recipients

We next studied the efficacy of I-CBP112 on leukemic cells isolated from mice transplanted with bone marrow retrovirally expressing fusion oncogenes (Fig. 5A; ref. 30). Treatment of primary murine MLL-AF9$^+$ leukemic blasts with I-CBP112 significantly impaired self-renewal in clonogenic replating assays in methylcellulose without significant cytotoxicity and induced significant morphologic cellular differentiation (Fig. 5B–D). Similar results were obtained in bone marrow cells *in vitro* immortalized by expression of the NUP98-HOXA9 or the MLL-AF9 fusion (Supplementary Fig. S4). The observation of reduced *in vitro* clonogenic growth (Fig. 5C) and absence of general toxicity (Fig. 5D) suggested that I-CBP112 might selectively reduce the number of leukemia-initiating cells (LIC) often also referred as leukemic stem cells. We therefore addressed the stem frequency of MLL-AF9–expressing blasts in methylcellulose by extreme limiting dilution analysis (ELDA; ref. 31) and found that treatment of the cells with 5 μmol/L I-CBP112 for 3 days resulted in a significant decrease in the estimated stem cell frequency (Fig. 5E).

In contrast to MLL-CBP, the MLL-AF9–driven mouse AML can be efficiently propagated by transplantation into irradiated recipient mice (30), making it an ideal model to study the antileukemic potential of CBP/p300 bromodomain inhibition *in vivo*. We first carried out a pharmacokinetic study in mice to assess suitability of I-CBP112 for progression into xenograft models. Intraperitoneal administration of the compound at 3 mg/kg yielded moderate systemic exposure of the compound with a mean C_{max} of 590 ng/mL [1.26 ± 0.74 μmol/L ($n = 3$)], an AUC of 384 ng/h/mL and a half-life of 0.6 ± 0.1 hours. Intravenous administration (1.2 mg/kg) revealed high blood clearance, moderate volume distribution, and comparison with intraperitoneal dosing suggested that I-CBP112 was bioavailable F%: 114 ± 63 $(AUC_t/D_{ip})/(AUC_\infty/D_{iv})$.

Because of the modest pharmacokinetic properties of I-CBP112, we used a pretreatment scheme to obtain a preliminary evaluation of I-CBP112 *in vivo* activity (Fig. 5A). I-CBP112 exposure of the cells for 3 days (5 μmol/L) in liquid cultures led to minor changes of expression of cell surface markers, only c-Kit/CD117 and granulocyte marker Gr-1 were slightly decreased (Supplementary Fig. S5).

We then compared disease initiation *in vivo* by transplanting I-CBP112 or DMSO pretreated MLL-AF9$^+$ AML cells in limited dilutions into secondary recipients. We observed that in doses from 5–50 × 10^3 cells, mice receiving treated cells developed the disease significantly later. Transplantation of as little as 500 control cells induced AML in all recipients after 50 days. In contrast, only 1 mouse transplanted with 500 I-CBP112–treated cells developed the disease only after a long latency (Fig. 5F and Supplementary Fig. S6). Collectively, these data demonstrate that exposure of murine MLL-AF9$^+$ leukemic blasts to the I-CBP112 CBP/p300 bromodomain inhibitor significantly reduced colony formation *in vitro*, as measured in the ELDA assay, and delayed induction of AML upon transplantation into irradiated recipients.

I-CBP112 impairs the clonogenic growth of human leukemic cells

To corroborate the observations made in the mouse model in the human disease, we screened a panel of 18 human leukemic cell lines for their sensitivity to I-CBP112. On the basis of the cancer cell line encyclopedia (CCLE), none of these cell lines harbor any mutations in the coding region of CBP or EP300 (Supplementary Table S4). Similar

(*Continued.*) B, cell-cycle phase distribution of KASUMI-1 cells analyzed by flow cytometry upon treatment with increasing doses of I-CBP112 at different time points. Medium and compound were renewed after 3 days. Shown is the mean percentage normalized to vehicle-treated control; error bars represent ±SD. *P* values are shown for G_1 phases and were calculated by using two-way ANOVA and Turkey multiple comparison; **, $P < 0.01$; ***, $P < 0.001$; ****, $P < 0.0001$; $n = 2$–4. C, clonogenic growth and cell numbers of primary blast cells from 5 AML patients. Shown is the mean percentage normalized to vehicle-treated control; error bars represent ±SD. *P* values were calculated by using ANOVA and Dunnett multiple comparison; **, $P < 0.01$; ***, $P < 0.001$; ****, $P < 0.0001$; $n = 5$. Morphology (Giemsa–Wright stain) of primary blast cells from AML patients treated with DMSO or 5 μmol/L I-CBP112. D, clonogenic growth and cell numbers of CD34$^+$ cells from healthy donors. Shown is the mean percentage normalized to vehicle-treated control; error bars represent ±SD. *P* values were calculated by using ANOVA and Dunnett multiple comparison; $n = 3$. Morphology (Giemsa-Wright stain) of CD34$^+$ cells from a healthy donor treated with DMSO or 5 μmol/L I-CBP112. E, synergy study of KASUMI-1, SEM, and MOLM13 cells treated either with indicated noncytotoxic doses of I-CBP112 (black bars), doxorubicin (gray bars), or both compounds (white bars). Concentrations used and combination index (CI) are given in the figure. CI < 1 indicates a synergistic effect. F, synergy study of KASUMI-1, SEM and MOLM13 cells treated either with indicated noncytotoxic doses of I-CBP112 (black bars), JQ1 (gray bars), or both compounds (white bars). Concentrations used and combination index (CI) are given in the figure. CI < 1 indicates a synergistic effect.

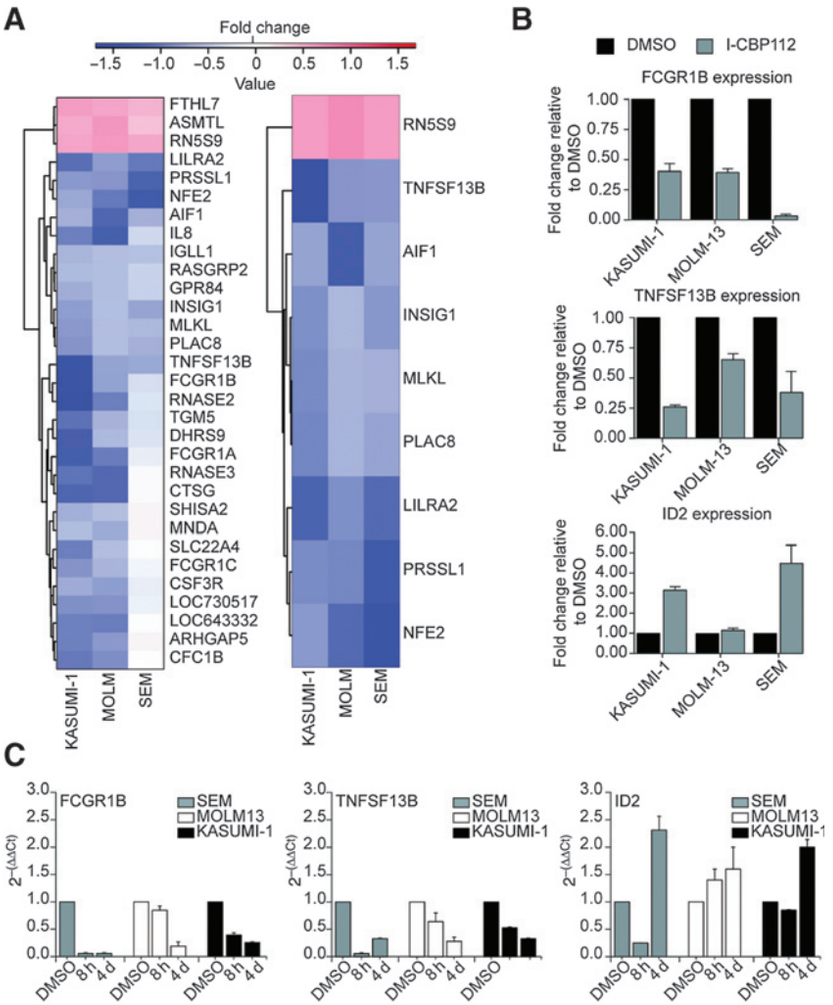

Figure 7.
I-CBP112 selectively modulates transcription. A, heatmap of selected genes. Shown are differences in gene transcription [$\log_2$(fold change)] color coded as indicated in the figure. B, confirmation of expression changes of selected genes that are regulated by I-CBP112 by qRT-PCR. C, time dependence of gene expression of selected genes monitored by qRT-PCR. Shown are average values of three biologic replicates.

to our observation on primary mouse leukemic blasts, we found that I-CBP112 did not cause immediate cytotoxic effects (Supplementary Figs. S7–S12). However, I-CBP112 significantly reduced the clonogenic growth in all 12 human cell lines that form visible colonies in methylcellulose (Supplementary Fig. S8). We selected three leukemic cell lines with distinct genetic lesions: KASUMI-1 (AML1-ETO$^+$), SEM (MLL-AF4$^+$), and MOLM13 (MLL-AF9$^+$/FLT3-ITD$^+$) for more detailed studies. I-CBP112 significantly impaired clonogenic growth of all three lines in a dose-dependent manner (Fig. 6A). I-CBP112 treatment resulted in dose-dependent G_1 arrest of the cell cycle. Time-dependent analysis of KASUMI-1 cells showed a prominent G_1 arrest at day 2 and 3 that was even more pronounced at day 6 (Fig. 6B). Prolonged exposure of cells to increasing concentrations of the compound in liquid culture resulted in signs of apoptosis (as measured by 7-AAD/AnnexinV staining) in KASUMI-1 cells at day 5, whereas MOLM13 and SEM were less sensitive (Supplementary Figs. S9–S11).

We also tested the effects of I-CBP112 on clonogenic growth of primary human cells. Exposure of cells from five different AML patients to I-CBP112 showed a dose-dependent reduction in the number of colonies and cells in methylcellulose. Similar to the murine and human leukemic cell lines, I-CBP112–treated primary AML cells showed morphologic signs of differentiation (Fig. 6C). In contrast, I-CBP112 exposure of peripheral CD34$^+$ cells from three healthy donors did not affect the colony number in methylcellulose. However, the size of the colonies was reduced, thus resulting in a statistically not significant tendency of lower overall cell numbers (Fig. 6D and Supplementary Fig. S12). These observations suggest that inhibition of the CBP/p300 bromodomain may have therapeutic potential in AML by suppressing self-renewal.

I-CBP112 sensitizes human leukemic cells to BET inhibition and doxorubicin

CBP/p300 and the BRD4 BET protein often colocalize on active promoters (32). However, in contrast to inhibition of BET bromodomains, blocking CBP/p300 BRDs by I-CBP112 resulted only in limited cytotoxicity. We therefore wondered whether exposure of combinations of both BRD inhibitors might show synergistic effects. In parallel, we also tested whether I-CBP112 might enhance cytotoxicity of doxorubicin, a clinically widely used genotoxic agent. We tested 8 different concentrations of I-CBP112 ranging from 0.1875 μmol/L to 24 μmol/L in combination with 15 different concentrations of JQ1 and doxorubicin, respectively, in ratios ranging from 8:1 to

1:16 in WST1 proliferation/survival assays for KASUMI-1, MOLM13, and SEM cells (Supplementary Fig. S12A and S12B). As expected, JQ1 and doxorubicin alone showed low nanomicromolar activity that was different for each of the three cell lines. We analyzed the potential synergistic activity using the Chou–Talalay method (33). We observed strong synergy combining either JQ1 or doxorubicin with I-CBP112 except for MOLM13 cells, in which synergism between doxorubicin and I-CBP112 was less pronounced (Fig. 6E and F and Supplementary Fig. S12C and S12D). We also compared the impact of these drug combinations on DNA damage by measuring γH2AX foci formation and H2AX Ser139 phosphorylation. In SEM and MOLM13, but not KASUM1 cells, increased γH2AX foci and H2AX Ser139 phosphorylation was seen after treatment with the I-CBP112/JQ1 combination. Exposure to doxorubicin increased H2Ax phosphorylation and foci that were not further increased by the combination with I-CBP112 (Supplementary Fig. S14). The combination of BET and CBP/p300 BRD inhibitors is of particular interest as both target subfamilies could be simultaneously targeted using a single agent with dual activity.

I-CBP112 modulates transcription of key inflammatory genes

To address the transcriptional consequences of exposure to I-CBP112, we performed microarray gene expression studies. We compared the gene expression signatures from KASUMI-1, MOLM13, and SEM leukemic cell lines that have been exposed to I-CBP112 for 4 days in liquid culture, a time point where cell-cycle alterations become detectable without any pronounced effects on cellular viability (Supplementary Fig. S7). Exposure of the three cell lines to I-CBP112 (3 μmol/L) resulted in transcriptional repression rather than activation. Unsupervised hierarchical clustering analysis identified significantly regulated genes. Heatmaps were generated for all genes identified as significantly altered (>1.5 FC, $P < 0.01$) in both KASUMI-1 and MOLM13 (Fig. 7A, left), or in all three of KASUMI-1, MOLM13, and SEM (Fig. 7A, right). Interestingly, many of the repressed genes were key regulators of immune response including the Fc fragment of IgG, high-affinity 1b, receptor (FCGR1B; CD64) playing an important role in humoral immune response (34), or TNFSF13B (B-cell–activating factor; B-lymphocyte stimulator; Delta4 BAFF) a member of the TNF ligand family (35). The expression changes of selected genes were confirmed by qRT-PCR (Fig. 7B) and found to be consistent with the array data. A list of all deregulated genes is compiled in Supplementary Tables S7–S9. To differentiate between early and late transcriptional changes, we measured mRNA levels at 8 hours and 4 days on a set of three representative deregulated genes identified in the array study (Fig. 7C). For the genes tested, stronger deregulation was observed after 4 days exposure to I-CBP112.

We used ChIP in combination with PCR to detect p300 levels in KASUMI-1 cells at promoter, enhancer, and exonic region of two significantly regulated genes: *TNFSF13B* and *ID2*. In agreement with our FRAP data, we did not see significant displacement of p300 after 8-hour exposure with 3 μmol/L I-CBP112. At longer exposure, however (4 days), we observed increased p300 occupancy at most regions investigated when compared with DMSO-treated cells, whereas control genes (IgG) were unaffected (Supplementary Fig. S16). Acetylation levels at p300/CBP substrate sites (H3K56ac, H3K56ac), which are also P300/CBP bromodomain–binding sites, were significantly reduced in particular after 4-day exposure to I-CBP112, suggesting that bromodomain inhibition affects also p300/CBP HAT activity at regulated gene promoters.

Discussion

High-resolution crystal structures allowed to rationally design several small molecules that selectively interact with high affinity to bromodomains of the BET family (19–22). BET inhibitors of the benzodiazepine scaffold gave rise to the inhibitor I-CBP112, the first selective and potent inhibitor developed for CBP/p300 bromodomains. Together with the HAT inhibitor C646 and inhibitors targeting other protein interaction domains the developed chemical probe extends the set of tool molecules targeting this key chromatin protein. Several studies demonstrated that BET inhibitors potently impaired the growth of cells originating from hematologic and solid cancers (22, 27, 36, 37). Analysis of a large number of different cell lines and primary murine and human cells revealed that I-CBP112 selectively impaired aberrant leukemic self-renewal. In contrast, BET inhibitors, such as JQ1 or PFI-1 potently impaired proliferation, survival, and self-renewal not only of cancer cells but also activated immune cells. This wide window of cellular activity might result from blocking interaction of BRD4 with a large number of super enhancer elements regulating multiple transcription factors including the Myc oncogene (38, 39). Not surprisingly, conditional ablation of BRD4 *in vivo* resulted in a severe phenotype due to stem cell depletion, for example, in the small intestine (40). Conditional ablation of *Cbp* in the hematopoietic system of adult mice led to an increase in differentiation, quiescence, apoptosis, and defects in adult HSC maintenance and self-renewal (5). Comparison with the observed cellular phenotypes induced by I-CBP112 observed in this study suggests that chemical inhibition of the CBP/p300 bromodomain phenocopies some but not all of the cellular effects observed in knockout studies including most remarkably defects in self-renewal and increased differentiation of immortalized hematopoietic cells as well as primary leukemic blasts. Reduction of colony formation by MLL-AF9–immortalized cells as shown by the ELDA assay *in vitro* and impaired disease induction by I-CBP112–treated leukemic blasts after transplantation strongly suggest significant activity of the compound on aberrant self-renewal of leukemic cells.

Domain-specific functions have recently been addressed in a systematic p300 deletion study in which loss of the p300 KIX or CH1 domains have been reported to cause profound defects in hematopoiesis, whereas deletion of other domains including the p300 bromodomain lead to lineage-restricted effects (41). Deletion of the bromodomain only modestly impaired p300 hematopoietic function in B cells but the bromodomain was required during T-cell development. Thus, the bromodomain interaction module may only be required for a subset of albeit critical fraction of CBP/p300 functions. Indeed, our FRAP and BRET experiments demonstrated that wild-type full-length CBP/p300 or mutants that lack the bromodomain interaction with acetylated histones remained bound to chromatin in the presence of I-CBP112. The lack of full displacement of CBP/p300 from chromatin may explain the modest effects of I-CBP112 on gene transcription in our microarray study that showed few genes upregulated greater than 2-fold after treatment with I-CBP112. The observed modest changes in gene transcription are however consistent with expression studies carried out using genetic deletion of CBP (5, 42, 43).

The small number of commonly regulated genes in all three cell lines tested was surprising, suggesting a strong context dependence of CBP/p300–regulated transcriptional events.

The role of CBP/p300 in human leukemogenesis is complex. Conditional knock-in of MLL-CBP in mice revealed that the fusion protein selectively expanded granulocyte/macrophage progenitors and enhanced their self-renewal/proliferation (44). In the MLL-CBP fusion, the bromo/HAT domain is maintained and required for the transforming activity of this oncogene (29). CBP/p300 was also found to regulate the transcriptional activity of the AML1-ETO fusion driving AML-M2 by posttranslational modification (12). CBP/p300 also seem to cooperate with the c-MYB proto-oncogene in cellular transformation by different leukemia-associated fusions including AML1-ETO, AML1-ETO9a, MLL-ENL, and MLL-AF9 (45). These observations suggest that the block of aberrant self-renewal in leukemic cells mediated by I-CBP112 might be the consequence of multiple activities influenced by the driver fusion oncogenes and multiple protein–protein interactions of CBP/p300. It has been estimated that CBP/p300 physically or functionally interact with close to 400 proteins acting as a coactivator of many transcription factors including NF-κB, HIF-1α, p53, or β-catenin that are known key regulators of leukemogenesis (46). It is likely that some of these interactions are influenced by the bromodomains. The p300 bromodomain for instance, has been reported to be required for recognition of specific acetylated lysine residues in p53 (47–49). We have recently observed that p53-dependent induction of the cell-cycle inhibitor p21 by genotoxic stress might be dependent on the CBP/p300 BRD. Interestingly we also found regulation of some p53 target genes at early time points in I-CBP112–treated KASUMI-1 leukemic cells (Supplementary Fig. S15). Hence, we found that the combination of I-CBP112 with doxorubicin resulted in significantly cytotoxicity in leukemic cells. Interestingly, we also saw also synergy between the BET inhibitor JQ1 and I-CBP112. Previous studies have shown synergistic cytotoxic activity of BET inhibitors with some HDAC inhibitors such as SAHA or LBH-589 in Myc induced murine lymphoma (50). Thus, small molecules CBP/p300 bromodomain inhibitors may have not only the potential to improve current therapies by selectively targeting aberrant self-renewal linked to disease relapse but also to enhance protocols combining BET inhibitors and traditional chemotherapy and suggest to further explore dual inhibitors targeting CBP/p300 and BET family bromodomains for their anticancer potential. Several compounds with dual BET and CBP/p300 activity have been developed in our laboratory demonstrating that selective targeting bromodomains of both bromodomain subfamilies is feasible using a single agent.

Disclosure of Potential Conflicts of Interest

No potential conflicts of interest were disclosed

Authors' Contributions

Conception and design: O. Fedorov, K. Jones, N. Parr, K. Lee, P. Jeffrey, P. Brennan, S. Muller, D. Hay, R. Prinjha, J. Schwaller, S. Knapp

Development of methodology: O. Fedorov, K. Leonards, M. Philpott, C. Wells, C. Bountra, P. Brennan, M. Urh, N.B. La Thangue, J. Schwaller

Acquisition of data (provided animals, acquired and managed patients, provided facilities, etc.): S. Picaud, O. Fedorov, A. Thanasopoulou, K. Leonards, K. Jones, H. Olzscha, S. Martin, A. Tumber, P. Filippakopoulos, K.H. Che, D. Lugo, S. Taylor, A. O'Mahony, S. Velichko, D.L. Daniels, N.B. La Thangue, R. Prinjha, J. Schwaller

Analysis and interpretation of data (e.g., statistical analysis, biostatistics, computational analysis): S. Picaud, O. Fedorov, A. Thanasopoulou, K. Leonards, K. Jones, H. Olzscha, O. Monteiro, M. Philpott, A. Tumber, P. Filippakopoulos, C. Wells, K.H. Che, A. Bannister, S. Robson, N. Parr, D. Lugo, P. Jeffrey, S. Taylor, M.L. Vecellio, P. Brennan, A. O'Mahony, S. Velichko, S. Muller, D.L. Daniels, N.B. La Thangue, J. Schwaller, S. Knapp

Writing, review, and/or revision of the manuscript: O. Fedorov, A. Thanasopoulou, K. Leonards, K. Jones, H. Olzscha, P. Filippakopoulos, C. Yapp, K.H. Che, A. Bannister, U. Kumar, P. Brennan, A. O'Mahony, S. Muller, R. Prinjha, J. Schwaller, S. Knapp

Administrative, technical, or material support (i.e., reporting or organizing data, constructing databases): K. Leonards, J. Meier, O. Monteiro, C. Yapp, N. Parr, C. Bountra, S. Muller

Study supervision: A. Bannister, U. Kumar, N. Parr, P. Jeffrey, C. Bountra, S. Muller, T. Kouzarides, R. Prinjha, J. Schwaller, S. Knapp

Other (made the figures displayed in the article): S. Picaud, O. Fedorov

Other (chemistry director with input and oversight of medicinal chemistry strategy and synthesis for GSK contribution): N. Parr

Other (codiscovery and characterization of the CBP inhibitor): R. Prinjha

Acknowledgments

The authors thank S. Juge and U. Schneider for providing technical support.

Grant Support

The SGC is a registered charity (number 1097737) that receives funds from the Canadian Institutes for Health Research, the Canada Foundation for Innovation, Genome Canada, GlaxoSmithKline, Pfizer, Eli Lilly, the Novartis Research Foundation, Takeda, Bayer, the Ontario Ministry of Research and Innovation, and the Wellcome Trust (092809/Z/10/Z]. P. Filippakopoulos and S. Picaud are supported by a Wellcome Trust Career Development Fellowship (095751/Z/11/Z). The work of the laboratory of J. Schwaller is supported by the Swiss National Science Foundation (SNF-31003A-130661/1), the Swiss Cancer League (KFS-3019-08-2012) and the Gertrude Von Meissner Foundation (Basel, Switzerland).

The costs of publication of this article were defrayed in part by the payment of page charges. This article must therefore be hereby marked *advertisement* in accordance with 18 U.S.C. Section 1734 solely to indicate this fact.

Received January 28, 2015; revised July 17, 2015; accepted August 7, 2015; published OnlineFirst November 9, 2015.

References

1. Chen J, Li Q. Life and death of transcriptional co-activator p300. Epigenetics 2011;6:957–61.
2. Delvecchio M, Gaucher J, Aguilar-Gurrieri C, Ortega E, Panne D. Structure of the p300 catalytic core and implications for chromatin targeting and HAT regulation. Nat Struct Mol Biol 2013;20:1040–6.
3. Kung AL, Rebel VI, Bronson RT, Ch'ng LE, Sieff CA, Livingston DM, et al. Gene dose-dependent control of hematopoiesis and hematologic tumor suppression by CBP. Genes Dev 2000;14:272–7.
4. Yao TP, Oh SP, Fuchs M, Zhou ND, Ch'ng LE, Newsome D, et al. Gene dosage-dependent embryonic development and proliferation defects in mice lacking the transcriptional integrator p300. Cell 1998;93:361–72.
5. Chan WI, Hannah RL, Dawson MA, Pridans C, Foster D, Joshi A, et al. The transcriptional coactivator Cbp regulates self-renewal and differentiation in adult hematopoietic stem cells. Mol Cell Biol 2011;31:5046–60.
6. Iyer NG, Ozdag H, Caldas C. p300/CBP and cancer. Oncogene 2004;23:4225–31.
7. Katsumoto T, Yoshida N, Kitabayashi I. Roles of the histone acetyltransferase monocytic leukemia zinc finger protein in normal and malignant hematopoiesis. Cancer Sci 2008;99:1523–7.
8. Zhang Y, Zeleznik-Le N, Emmanuel N, Jayathilaka N, Chen J, Strissel P, et al. Characterization of genomic breakpoints in MLL and CBP in leukemia patients with t(11;16). Genes Chromosomes Cancer 2004;41:257–65.

9. Rowley JD, Reshmi S, Sobulo O, Musvee T, Anastasi J, Raimondi S, et al. All patients with the T(11;16)(q23;p13.3) that involves MLL and CBP have treatment-related hematologic disorders. Blood 1997;90:535–41.
10. Kasper LH, Brindle PK, Schnabel CA, Pritchard CE, Cleary ML, van Deursen JM. CREB binding protein interacts with nucleoporin-specific FG repeats that activate transcription and mediate NUP98-HOXA9 oncogenicity. Mol Cell Biol 1999;19:764–76.
11. Zhao Y, Lu S, Wu L, Chai G, Wang H, Chen Y, et al. Acetylation of p53 at lysine 373/382 by the histone deacetylase inhibitor depsipeptide induces expression of p21(Waf1/Cip1). Mol Cell Biol 2006;26:2782–90.
12. Wang L, Gural A, Sun XJ, Zhao X, Perna F, Huang G, et al. The leukemogenicity of AML1-ETO is dependent on site-specific lysine acetylation. Science 2011;333:765–9.
13. Arif M, Pradhan SK, Thanuja GR, Vedamurthy BM, Agrawal S, Dasgupta D, et al. Mechanism of p300 specific histone acetyltransferase inhibition by small molecules. J Med Chem 2009;52:267–77.
14. Santer FR, Hoschele PP, Oh SJ, Erb HH, Bouchal J, Cavarretta IT, et al. Inhibition of the acetyltransferases p300 and CBP reveals a targetable function for p300 in the survival and invasion pathways of prostate cancer cell lines. Mol Cancer Ther 2011;10:1644–55.
15. Gao XN, Lin J, Ning QY, Gao L, Yao YS, Zhou JH, et al. A histone acetyltransferase p300 inhibitor C646 induces cell cycle arrest and apoptosis selectively in AML1-ETO-positive AML cells. PLoS One 2013;8:e55481.
16. Borah JC, Mujtaba S, Karakikes I, Zeng L, Muller M, Patel J, et al. A small molecule binding to the coactivator CREB-binding protein blocks apoptosis in cardiomyocytes. Chem Biol 2011;18:531–41.
17. Hewings DS, Wang M, Philpott M, Fedorov O, Uttarkar S, Filippakopoulos P, et al. 3,5-dimethylisoxazoles act as acetyl-lysine-mimetic bromodomain ligands. J Med Chem 2011;54:6761–70.
18. Vidler LR, Brown N, Knapp S, Hoelder S. Druggability analysis and structural classification of bromodomain acetyl-lysine binding sites. J Med Chem 2012;55:7346–59.
19. Filippakopoulos P, Qi J, Picaud S, Shen Y, Smith WB, Fedorov O, et al. Selective inhibition of BET bromodomains. Nature 2010;468:1067–73.
20. Nicodeme E, Jeffrey KL, Schaefer U, Beinke S, Dewell S, Chung CW, et al. Suppression of inflammation by a synthetic histone mimic. Nature 2010;468:1119–23.
21. Picaud S, Da Costa D, Thanasopoulou A, Filippakopoulos P, Fish PV, Philpott M, et al. PFI-1, a highly selective protein interaction inhibitor, targeting BET Bromodomains. Cancer Res 2013;73:3336–46.
22. Dawson MA, Prinjha RK, Dittmann A, Giotopoulos G, Bantscheff M, Chan WI, et al. Inhibition of BET recruitment to chromatin as an effective treatment for MLL-fusion leukaemia. Nature 2011;478:529–33.
23. Fedorov O, Niesen FH, Knapp S. Kinase inhibitor selectivity profiling using differential scanning fluorimetry. Methods Mol Biol 2012;795:109–18.
24. Philpott M, Yang J, Tumber T, Fedorov O, Uttarkar S, Filippakopoulos P, et al. Bromodomain-peptide displacement assays for interactome mapping and inhibitor discovery. Mol Biosyst 2011;7:2899–908.
25. Filippakopoulos P, Picaud S, Fedorov O, Keller M, Wrobel M, Morgenstern O, et al. Benzodiazepines and benzotriazepines as protein interaction inhibitors targeting bromodomains of the BET family. Bioorg Med Chem 2012;20:1878–86.
26. Philpott M, Rogers CM, Yapp C, Wells C, Lambert JP, Strain-Damerell C, et al. Assessing cellular efficacy of bromodomain inhibitors using fluorescence recovery after photobleaching. Epigenetics Chromatin 2014;7:14.
27. Ciceri P, Muller S, O'Mahony A, Fedorov O, Filippakopoulos P, Hunt JP, et al. Dual kinase-bromodomain inhibitors for rationally designed polypharmacology. Nat Chem Biol 2014;10:305–12.
28. Hay DA, Fedorov O, Martin S, Singleton DC, Tallant C, Wells C, et al. Discovery and optimization of small-molecule ligands for the CBP/p300 bromodomains. J Am Chem Soc 2014;136:9308–19.
29. Lavau C, Du C, Thirman M, Zeleznik-Le N. Chromatin-related properties of CBP fused to MLL generate a myelodysplastic-like syndrome that evolves into myeloid leukemia. EMBO J 2000;19:4655–64.
30. Mereau H, De Rijck J, Cermakova K, Kutz A, Juge S, Demeulemeester J, et al. Impairing MLL-fusion gene-mediated transformation by dissecting critical interactions with the lens epithelium-derived growth factor (LEDGF/p75). Leukemia 2013;27:1245–53.
31. Hu Y, Smyth GK. ELDA: extreme limiting dilution analysis for comparing depleted and enriched populations in stem cell and other assays. J Immunol Methods 2009;347:70–8.
32. Reynoird N, Schwartz BE, Delvecchio M, Sadoul K, Meyers D, Mukherjee C, et al. Oncogenesis by sequestration of CBP/p300 in transcriptionally inactive hyperacetylated chromatin domains. EMBO J 2010;29:2943–52.
33. Chou TC. Drug combination studies and their synergy quantification using the Chou-Talalay method. Cancer Res 2010;70:440–6.
34. Sutherland JS, Loxton AG, Haks MC, Kassa D, Ambrose L, Lee JS, et al. Differential gene expression of activating Fcgamma receptor classifies active tuberculosis regardless of human immunodeficiency virus status or ethnicity. Clin Microbiol Infect 2014;20:O230–8.
35. Thompson JS, Bixler SA, Qian F, Vora K, Scott ML, Cachero TG, et al. BAFF-R, a newly identified TNF receptor that specifically interacts with BAFF. Science 2001;293:2108–11.
36. Filippakopoulos P, Knapp S. Targeting bromodomains: epigenetic readers of lysine acetylation. Nat Rev Drug Discov 2014;13:337–56.
37. Zuber J, Shi J, Wang E, Rappaport AR, Herrmann H, Sison EA, et al. RNAi screen identifies Brd4 as a therapeutic target in acute myeloid leukaemia. Nature 2011;478:524–8.
38. Shi J, Vakoc CR. The mechanisms behind the therapeutic activity of BET bromodomain inhibition. Mol Cell 2014;54:728–36.
39. Delmore JE, Issa GC, Lemieux ME, Rahl PB, Shi J, Jacobs HM, et al. BET bromodomain inhibition as a therapeutic strategy to target c-Myc. Cell 2011;146:904–17.
40. Bolden JE, Tasdemir N, Dow LE, van Es JH, Wilkinson JE, Zhao Z, et al. Inducible in vivo silencing of Brd4 identifies potential toxicities of sustained BET protein inhibition. Cell Rep 2014;8:1919–29.
41. Kimbrel EA, Lemieux ME, Xia X, Davis TN, Rebel VI, Kung AL. Systematic in vivo structure-function analysis of p300 in hematopoiesis. Blood 2009;114:4804–12.
42. Kang-Decker N, Tong C, Boussouar F, Baker DJ, Xu W, Leontovich AA, et al. Loss of CBP causes T cell lymphomagenesis in synergy with p27Kip1 insufficiency. Cancer Cell 2004;5:177–89.
43. Xu W, Fukuyama T, Ney PA, Wang D, Rehg J, Boyd K, et al. Global transcriptional coactivators CREB-binding protein and p300 are highly essential collectively but not individually in peripheral B cells. Blood 2006;107:4407–16.
44. Wang J, Iwasaki H, Krivtsov A, Febbo PG, Thorner AR, Ernst P, et al. Conditional MLL-CBP targets GMP and models therapy-related myeloproliferative disease. EMBO J 2005;24:368–81.
45. Pattabiraman DR, McGirr C, Shakhbazov K, Barbier V, Krishnan K, Mukhopadhyay P, et al. Interaction of c-Myb with p300 is required for the induction of acute myeloid leukemia (AML) by human AML oncogenes. Blood 2014;123:2682–90.
46. Mendonca DB, Mendonca G, Cooper LF. Mammalian two-hybrid assays for studies of interaction of p300 with transcription factors. Methods Mol Biol 2013;977:323–38.
47. Wei L, Jamonnak N, Choy J, Wang Z, Zheng W. Differential binding modes of the bromodomains of CREB-binding protein (CBP) and p300 with acetylated MyoD. Biochem Biophys Res Commun 2008;368:279–84.
48. Hou T, Ray S, Lee C, Brasier AR. The STAT3 NH2-terminal domain stabilizes enhanceosome assembly by interacting with the p300 bromodomain. J Biol Chem 2008;283:30725–34.
49. Mujtaba S, He Y, Zeng L, Yan S, Plotnikova O, Sachchidanand, et al. Structural mechanism of the bromodomain of the coactivator CBP in p53 transcriptional activation. Mol Cell 2004;13:251–63.
50. Bhadury J, Nilsson LM, Muralidharan SV, Green LC, Li Z, Gesner EM, et al. BET and HDAC inhibitors induce similar genes and biological effects and synergize to kill in Myc-induced murine lymphoma. Proc Natl Acad Sci U S A 2014;111:E2721–30.